symmetry

MDPI

Article

Self-Diffusiophoresis and Symmetry-Breaking of a Janus Dimer: Analytic Solution

Eldad J. Avital [1] and Touvia Miloh [2,*]

[1] School of Engineering and Materials Science, Queen Mary University of London, London E1 4NS, UK; e.avital@qmul.ac.uk
[2] School of Mechanical Engineering, Tel Aviv University, Tel Aviv 69978, Israel
* Correspondence: miloh@eng.tau.ac.il

Abstract: A self-diffusiophoretic problem is considered for a chemically active dimer consisting of two equal touching spherical colloids that are exposed to different fixed-flux and fixed-rate surface reactions. A new analytic solution for the autophoretic mobility of such a catalytic Janus dimer is presented in the limit of a small Péclet number and linearization of the resulting Robin-type boundary value problem for the harmonic solute concentration. Explicit solutions in terms of the physical parameters are first obtained for the uncoupled electrostatic and hydrodynamic problems. The dimer mobility is then found by employing the reciprocal theorem depending on the surface slip velocity and on the normal component of the shear stress acting on the inert dimer. Special attention is given to the limiting case of a Janus dimer composed of an inert sphere and a chemically active sphere where the fixed-rate reaction (Damköhler number) is infinitely large. Examples are given, comparing the numerical and approximate analytic solutions of the newly developed theory. Singular points arising in the model are discussed for a dimer with a fixed-rate reaction, and the flow field around the dimer is also analysed. The new developed theory introduces a fast way to compute the mobility of a freely suspended dimer and the induced flow field around it, and thus can also serve as a sub grid scale model for a multi-scale flow simulation.

Keywords: self-diffusiophoresis; dimer and tangent-sphere coordinates; chemically-active Janus; symmetry-breaking; electrokinetics

Citation: Avital, E.J.; Miloh, T. Self-Diffusiophoresis and Symmetry-Breaking of a Janus Dimer: Analytic Solution. *Symmetry* **2023**, *15*, 2019. https://doi.org/10.3390/sym15112019

Academic Editor: Toshio Tagawa

Received: 10 October 2023
Revised: 27 October 2023
Accepted: 31 October 2023
Published: 3 November 2023

1. Introduction

The subject of autophoretic mobility of active colloids (rigid or deformable) continues to attract attention within the nano-technology community, for example, in recent reviews [1,2]. Among the various physical/chemical mechanisms related to the self-propulsion problem of freely suspended micron-size particles in an unbounded solute in the absence of any external forcing [3–5], we chose here self-diffusiophoresis as an archetypal problem [6–8]. Within this framework, particle mobility is deduced by a symmetry-breaking effect resulting from different types of surface on the two spheres. The first is a fixed-flux (absorption/release) mechanism and the other is a fixed-rate one-step chemical reaction [8]. In the limiting case of a small Péclet number, i.e., when advection is considered small with respect to diffusion, the governing equation for the solute concentration is governed by the Laplace equation and is subject to a mixed (Robin-type) boundary condition on the colloid's surface together with a proper far-field limit.

There is a vast body of literature on self-propulsion of capped Janus spherical colloids arising due to material/chemical symmetry-breaking which can be modelled by applying disparate boundary conditions over different parts of the surface [9–16], typically with a symmetric Janus composed of two hemispheres. However, other three-dimensional (3D) geometries that can be analytically handled are, for example, convex separable shapes, such as ellipsoidal and spheroidal particles (slender rods and elliptic discs as limiting

cases) [17–23]. Note that for such simple autotropic shapes (possessing three planes of symmetry), the self-phoretic mobility can be directly found (under the assumption of a thin reaction layer [8]) in terms of the induced surface slip velocity [24] without using the reciprocal theorem [25]. This involves resolving the hydrodynamic (Stokes) problem and finding the shear stress over a uniformly translating inert particle. Note that for a perfectly symmetric spherical colloid suspended in a free space, the autophoretic mobility can be directly obtained by calculating the average of the slip velocity over the particle surface. However, such a simple averaging procedure does not hold, for example, in the present dimer configuration (pair interaction).

The self-diffusiophoresis problem between two chemically active interacting spherical colloids is also amenable to analysis by employing a separable bi-spherical coordinate system [26–28]. Identical chemical activity is assumed on the two adjacent spheres and self-propulsion is a result of geometric asymmetry (different radii). An induced mobility of two interacting spheres (dumbbell) can also result from applying different chemical activities on two spheres of the same size [29]. A constant fixed reaction has been assumed on the spherical spheres [26–30]. A special Janus dimer (JD) configuration is that of two identical touching spheres possessing distinct chemical surface activities, which is again amenable to analysis using a separable 3D orthogonal tangent-sphere coordinate system [31]. In contrast to the bi-spherical (BS) system, the tangent-sphere (TS) curvilinear system admits a more direct and compact integral formulation (as compared to infinite summation in BS) and was found useful in obtaining explicit solutions for some related electrostatic problems [32].

Motivated by the recent advent in self-propelling platforms, such as micro/nano motors with the capability of effectively transforming surface chemical energy into mechanical energy resulting in phoretic motions [33–35], we consider here the self-diffusiophoresis problem of a chemically active spherical Janus dimer and obtain explicit expressions for the dimer mobility. By employing the extended Robin-type boundary condition on the two spheres, corresponding to using distinct values for the fixed-rate and fixed-flux parameters [8], we obtain explicit solutions for the autophoretic mobility of a Janus dimer in terms of the chemical (fixed-flux and fixed-rate) reactions prevailing over the two spheres. Finally, following ref. [16], we consider the special interesting case of a dimer-motor composed of an inert sphere and a chemically active sphere in the limit of an infinitely large Damköhler number [8] and derive a simple practical analytic expression for its self-diffusiophoretic velocity which may serve as a benchmark solution.

It should be noted that in large-scale applications, effects from adjacent dimers or nearby walls may be influential on the motion of the dimer. Contact between heterogenous parts of different dimers can lead to collective behaviour and to convoluted motion with six degrees of freedom. Noticeable numerical and analytical studies of interacting colloids of different shapes of heterogeneous chemical and electrical properties have been carried out. This includes for example investigating the effect of colloid's geometry (e.g., sphere/rod [36]), solid particle and gas bubble interaction in a liquid medium [37], motion of a large set of charged particles [38]. The present study, which focuses on a single free dimer, can be considered as an interaction between two (identical) touching spherical colloids forming a dimer, where the effect of nearby particles and boundaries is left for future study.

The structure of the paper is as follows: The problem formulation is presented in the Materials and Methods under Section 2.1 for a general free catalytic Janus dimer in the limit of a small Péclet number and a thin interaction layer [8], by employing the integral tangent-sphere formulation [32]. The solute concentration is shown to be governed by the Laplace Equation and by a mixed (Robin-type) boundary condition applied on the dimer's surface. A proper solution for the harmonic concentration is presented in Section 2.2 by means of solving two coupled ordinary differential equations. Some exact solutions are also compared against the obtained numerical and asymptotic solutions. An integral expression for the induced slip velocity on the dimer's surface is then presented obtained in Section 2.3 by employing a special variant of using the reciprocal theorem [25].

This procedure requires solving the Stokes (low-Reynolds) hydrodynamic problem of a uniformly translating inert dimer in order to determine the corresponding shear stress component over its surface as presented in Section 2.4. An explicit solution is then derived for the autophoretic mobility of such a Janus dimer as well as for the Stokes stream function of a self-propelled catalytic dimer. Finally, we provide a simple explicit expression for the mobility of a dimer composed of an inert sphere and a chemically active sphere in the limit of a very large Damköhler number [16] in Section 2.5. We follow with a discussion of the analytic results thus found, including a comparison against numerical computations and asymptotic approximations including a short conclusion section. A list of the main symbols is presented after Section 4, followed by Appendix A detailing the numerical procedure developed to solve the coupled ordinary differential equations derived in order to compute the dimer mobility and the flow field around it.

2. Materials and Methods

2.1. Problem Formulation

We consider a catalytic Janus dimer (JD) consisting of two touching rigid chemically active spheres of the same size, freely suspended in an unbounded symmetric electrolyte of dynamic viscosity K, diffusivity k, and ambient concentration C_∞. For simplicity, we consider all parameters as constants. The two spherical surfaces (possessing different surface activity) are denoted here by $S_\pm$, (see Figure 1). Under the assumption of a small Péclet number and a thin interaction layer [8], the linearised solution for the solute concentration C (normalised by C_∞) is governed by the Laplace Equation $\nabla^2 C = 0$ and a mixed (Robin-type) boundary condition applied on the two dimer surfaces ($S_\pm$):

$$\frac{\partial C}{\partial n} = -\alpha_\pm + \beta_\pm C \text{ on } S_\pm. \tag{1}$$

which is subject to $C \to 1$ in the far-field. Here, $\partial/\partial n$ denotes the outward normal derivative to the dimer surface and the four dimensional parameters $(\alpha_\pm, \beta_\pm)$ represent the corresponding chemical activities on $S_\pm$. Following Michelin and Lauga [8], α represents the "fixed-flux" parameter whereas β is the so-called "fixed-rate" parameter which is also associated with the Damköhler number (the ratio between the diffusivity and reactive time scales). Note that for a chemically active JD the four parameters $(\alpha_\pm, \beta_\pm)$ are generally different. However, if one of the surfaces $S_\pm$ is chemically inactive (inert), then the corresponding parameters of (α, β) vanish, and Equation (1) reduces on that surface to the homogenous Neumann boundary condition, i.e., $\partial C/\partial n = 0$.

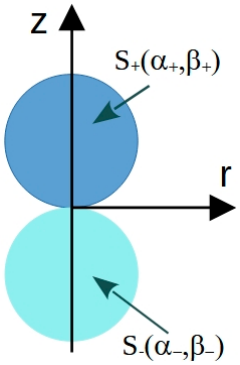

Figure 1. Schematic description of the dimer composed of two spheres of the same size but of different surface activities, where the dimer is freely suspended in an unbounded symmetric electrolyte of dynamic viscosity K, diffusivity k, and ambient concentration C_∞.

The self-diffusiophoretic mobility of the JD depends on the velocity slip induced on the surfaces $S_\pm$, which following [39] can be expressed as

$$\vec{u_s} = M_\pm \nabla_{||} C, \tag{2}$$

where $M_{\pm}$ denotes the mobility coefficients on $S_{\pm}$ respectively and $\nabla_{||}$ represents the surface tangential derivative. Our task here is to obtain an explicit (analytic) expression for the self-diffusiophoretic mobility of a general active JD in terms of the six parameters $(\alpha_{\pm}, \beta_{\pm}, M_{\pm})$, including the JD radius (a) and solute viscosity (K). Note that the solute diffusivity (k) and the ambient concentration (C_{∞}) are already included in the normalised parameters $(\alpha_{\pm}, \beta_{\pm})$.

Taking advantage of the axisymmetric nature of the physical problem with respect to the line of centres (z axis), it is convenient to employ here a semi-separable tangential-sphere system (μ, υ), which is related to a cylindrical system (r, z) by the following transformation [31,32]:

$$r = \frac{\mu}{\mu^2 + \upsilon^2}, \; z = \frac{\upsilon}{\mu^2 + \upsilon^2}, \tag{3}$$

where $\mu \in [0, \infty]$ and $\upsilon \in [0, \infty]$. Note that (r, z) in Equation (3) are normalised with respect to the diameter of the two spheres ($2a$). In addition, the surface of the upper surface (see Figure 1) namely $z > 0$ is given by $\upsilon = 1$, whereas the surface of the lower surface ($z < 0$) is represented by $\upsilon = -1$. The corresponding surfaces of the two spheres composing the dimer are thus denoted by $S_{\pm}$ with the corresponding parameters of $(\alpha_{\pm}, \beta_{\pm}, M_{\pm})$.

2.2. Solute Concentration

Bearing in mind that the solute concentration $C(\mu, \upsilon)$ is a harmonic function satisfying $C \to 1$ at infinity, one can write [32]:

$$C(\mu, \upsilon) = 1 + \left(\mu^2 + \upsilon^2\right)^{1/2} \int_0^{\infty} [A(s)cosh(s\upsilon) + B(s)sinh(s\upsilon)] J_0(s\mu) ds, \tag{4}$$

where $J_n(s)$ denotes the Bessel function of order n, and the coefficients $A(s)$ and $B(s)$ can be found by satisfying Equation (1). Thus, substituting Equation (4) into Equation (1) and noting that $\partial/\partial n = \left(1 + \mu^2\right)^{-1} \partial/\partial \upsilon$ on $S_{\pm}$, i.e., at $\upsilon = \pm 1$ respectively, one gets:

$$\begin{array}{c} \pm A(s)cosh(s) + B(s)sinh(s) \pm [A(s)sinh(s) \pm B(s)cosh(s)] \\ \mp \frac{d}{dS}\left\{ s \frac{d}{ds} [A(s)sinh(s) \pm B(s)cosh(s)] \right\} = \\ -(\alpha_{\pm} - \beta_{\pm}) e^{-s} + \beta_{\pm} [A(s)cosh(s) \mp B(s)sinh(s)] \end{array} . \tag{5}$$

When deriving Equation (5) we used the following identity [40]:

$$1/\left(\mu^2 + \upsilon^2\right)^{1/2} = \int_0^{\infty} e^{-s|\upsilon|} J_0(s\mu) ds. \tag{6}$$

Finally, Equation (5) is actually two equations that can be written as:

$$\begin{array}{c} \frac{1}{sinh(s)} \frac{d}{ds} \left[s \times sinh^2(s) \frac{dA(s)}{ds} \right] + \frac{\beta_+ - \beta_-}{2} A(s)cosh(s) + \frac{\beta_+ + \beta_-}{2} B(s)sinh(s) \\ = \frac{e^{-s}}{2} [(\alpha_+ - \alpha_-) - (\beta_+ - \beta_-)] \end{array} \tag{7a}$$

$$\begin{array}{c} \frac{1}{cosh(s)} \frac{d}{ds} \left[s \times cosh^2(s) \frac{dB(s)}{ds} \right] + \frac{\beta_+ - \beta_-}{2} B(s)sinh(s) + \frac{\beta_+ + \beta_-}{2} A(s)cosh(s) \\ = \frac{e^{-s}}{2} [(\alpha_+ - \alpha_-) - (\beta_+ - \beta_-)] \end{array} . \tag{7b}$$

It is interesting to note that for the special case where $(\beta_{\pm} = 0)$, namely for a fixed-flux reaction, a first integral can be found for Equation (7) resulting in:

$$\frac{dA(s)}{ds} = \frac{\alpha_+ - \alpha_-}{4} \times \frac{s - e^{-s} sinh(s)}{s \times sinh^2(s)}, \; \frac{dB(s)}{ds} = \frac{\alpha_+ + \alpha_-}{4} \times \frac{s + e^{-s} sinh(s)}{s \times cosh^2(s)} \tag{8}$$

which can be solved by numerical integration. One should note the singularity of $A(s)$ at $s = 0$, behaving as $\log(s)$ where $B(s)$ is finite at $s = 0$. Both $A(s \to \infty)$ and $B(s \to \infty)$ approach zero, making the integration of Equation (8) well defined.

Equation (7) can be solved numerically by discretising it using staggered central finite differences [41], and employing a block matrix tri-diagonal solver as further detailed in Appendix A. The asymptotic solution of Equation (7) for large s yields:

$$A(s) = \frac{\gamma_+(\beta_+ + \beta_-) - \gamma_-(\beta_+ - \beta_- - 4)}{2(\beta_+ - 2)(\beta_- + 2)} e^{-2s},\ B(s) = \frac{\gamma_-(\beta_+ + \beta_-) - \gamma_+(\beta_+ - \beta_- - 4)}{2(\beta_+ - 2)(\beta_- + 2)} e^{-2s}, \tag{9}$$

where

$$\gamma_\pm = (\alpha_+ \pm \alpha_-) - (\beta_+ \pm \beta_-). \tag{10}$$

Note that for $\beta_\pm = 0$, Equation (9) yields $A(s) = -(\alpha_+ - \alpha_-)e^{-2s}/2$ and $B(s) = -(\alpha_+ + \alpha_-)e^{-2s}/2$ in agreement with Equation (8) under the limit $s \to \infty$.

2.3. Velocity Slip

The slip velocity on the JD can be expressed following Equations (2) and (4) as $\vec{u}_s = M_\pm u_\pm \hat{e}_\mu$ where

$$u_\pm(\mu) = \left(1 + \mu^2\right) \frac{\partial}{\partial \mu} \left[\left(1 + \mu^2\right)^{1/2} \int_0^\infty F_{\pm -}(s) J_0(s\mu) ds \right] \text{ on } S_\pm, \tag{11}$$

and

$$F_\pm(s) = A(s) cosh(s) \pm B(s) sinh(s). \tag{12}$$

Here $\hat{e}_\mu$ denotes a unit vector along the curvilinear coordinate μ. Integration by parts of Equation (11) renders:

$$u_\pm(\mu) = \frac{\left(1 + \mu^2\right)^{1/2}}{\mu} \left\{ \mu^2 \int_0^\infty \left[\frac{d}{ds}(sF_\pm(s) J_0(s\mu)) - s \frac{dF_\pm(s)}{ds} J_0(s\mu) \right] ds + \int_0^\infty sF_\pm(s) \frac{dJ_0(s\mu)}{ds} ds \right\}. \tag{13}$$

The integral of the first term on the right hand side (RHS) of Equation (13) vanishes and since $s\mu^2 J_0(s\mu) = -sd[sdJ_0(s\mu)/ds]/ds$, Equation (13) reduces to

$$u_\pm(\mu) = \left(1 + \mu^2\right)^{1/2} \int_0^\infty sG_\pm(s) J_0(s\mu) ds, \tag{14}$$

where

$$G_\pm(s) = \frac{d^2 F_\pm(s)}{ds^2} - F_\pm(s) = \frac{1}{cosh(s)} \frac{d}{ds} \left[cosh^2(s) \frac{dA(s)}{ds} \right] \pm \frac{1}{sinh(s)} \frac{d}{ds} \left[sinh^2(s) \frac{dB(s)}{ds} \right]. \tag{15}$$

It is important to note that $G_\pm(s)$, which determines the slip velocity on the JD by means of Equation (14), is expressed in terms of the first derivatives of $A(s)$ and $B(s)$, thus enabling us to directly use Equation (8) for the fixed-flux case.

Once the slip velocity $u_\pm(\mu)$ of Equation (14) on the dimer's surface is known, the self-diffusiophoretic mobility of the JD can be expressed by means of the reciprocal theorem for Stokes flows [25] in terms of the tangential component of the normal shear stress $\sigma_{\mu v}(\mu, \pm 1)$ exerted on an inert dimer moving with a unit velocity along the line of centres (z axis). Thus, following [28] the dimer mobility velocity (along the z axis of symmetry) is given by:

$$U_{\mathrm{d}} = \sum \frac{M_\pm}{D_v} \int_{S_\pm} u_\pm(s) \sigma_{\mu v}(\mu, \pm 1) dS,\ dS = \frac{2\pi \mu d\mu}{\left(1 + \mu^2\right)^2}, \tag{16}$$

where $S = S_+ \cup S_-$, $\sum$ represent a sum over S_+ and S_-, and D_v denotes the drag acting on the inert dimer moving with unit velocity in the z direction.

What remains is to find the hydrodynamic shear stress component $\sigma_{\mu v}(\mu, \pm 1)$ of a chemically inactive (inert) rigid dimer translating along its axis of symmetry, as demonstrated in the following section.

2.4. Hydrodynamic Problem of an Inert Dimer

In order to find the mobility of a chemically active JD by means of the reciprocal theorem and Equation (16), one needs first to solve the hydrodynamic problem of an inert dimer moving with a unit velocity in the z direction (axis of symmetry). Assuming creeping (Stokes) flow of an incompressible fluid, the velocity field $\vec{u}(r,z)$ and the hydrodynamic pressure $p(r,z)$, expressed in body attached cylindrical coordinate system, are governed by

$$K\nabla^2\vec{u} = \nabla p,\ \nabla\cdot\vec{u} = 0, \tag{17}$$

subject to $\vec{u} = 0$ on S and $\vec{u}\cdot\hat{e}_z = -1$ together with $p = 0$ far from the body.

Following [42,43] the tangent-sphere coordinate system was employed along with a stream function formulation $\Psi(\mu,v)$, where the corresponding velocity components $u_\mu(\mu,v)$ and $u_v(\mu,v)$ are given by:

$$u_\mu(\mu,v) = \frac{\left(\mu^2+v^2\right)^2}{\mu}\frac{\partial\Psi(\mu,v)}{\partial v},\ u_v(\mu,v) = -\frac{\left(\mu^2+v^2\right)^2}{\mu}\frac{\partial\Psi(\mu,v)}{\partial\mu}, \tag{18}$$

where

$$\Psi(\mu,v) = \frac{1}{2}\frac{\mu^2}{\left(\mu^2+v^2\right)^2} + \frac{\mu}{\left(\mu^2+v^2\right)^{3/2}}\int_0^\infty H(s,v)J_1(s\mu)ds, \tag{19}$$

and

$$H(s,v) = C(s)\cos h(sv) + vD(s)\sin h(sv). \tag{20}$$

The two coefficients $C(s)$ and $D(s)$ in Equations (19) and (20) can be readily found by applying the no-slip and no-penetration boundary conditions on the dimer surface $(v=\pm1)$, namely $\Psi(\mu,\pm1) = 0$ and $\partial\Psi(\mu,\pm1)/\partial v = 0$, leading to [43]:

$$C(s) = -\frac{1+s+e^{-2s}sinh(2s)/s}{2s+sinh(2s)},\ D(s) = \frac{s+e^{-s}\sin hs}{2s+sinh(2s)}. \tag{21}$$

Once the stream function and the velocity components of Equation (18) are known one can calculate the normal shear component $\sigma_{\mu v}(\mu,\pm1)$ exerted on the dimer surface as [44–46]:

$$\frac{\sigma_{\mu v}(\mu,\pm1)}{K} = \frac{\partial}{\partial\mu}\left(\frac{u_v}{h_\mu}\right) + \frac{\partial}{\partial v}\left(\frac{u_\mu}{h_v}\right), \tag{22}$$

where the corresponding metric coefficients in Equation (22) are given by $h_\mu = h_v = \left(\mu^2+v^2\right)^{-1}$. Next, since $u_v = \left(\partial u_\mu\right)/(\partial\mu) = 0$ on $v=\pm1$, Equations (18) and (22) yield:

$$\frac{\sigma_{\mu v}(\mu,\pm1)}{K} = \frac{1}{h_v}\frac{\partial u_\mu}{\partial v} = \frac{\left(1+\mu^2\right)^3}{\mu}\frac{\partial^2\Psi(\mu,\pm1)}{\partial v^2}, \tag{23}$$

substituting Equation (19) into Equation (23) renders:

$$\frac{\sigma_{\mu v}(\mu,\pm1)}{K} = -\frac{\mu}{2} + \frac{3\mu}{2(1+\mu^2)} + \left(1+\mu^2\right)^{3/2}\int_0^\infty I(s)J_1(\mu s)ds, \tag{24}$$

whereby Equation (21):

$$\begin{aligned} I(s) &= s^2[C(s)cosh(s) + D(s)sinh(s)] + 2sD(s)cosh(s) \\ &= -\tfrac{s}{2}e^{-s}(1+s) + \tfrac{2s\left[s+e^{-s}sinh(s)\right]}{2s+sinh(2s)} \end{aligned} \tag{25}$$

Finally, the viscous drag D_v exerted on the inert dimer can be computed by means of the stream function formulation of [42,43] which leads to:

$$D_v = -6\pi Kf,\ f = \frac{2}{3}\int_0^\infty sC(s)ds \simeq 0.645, \tag{26}$$

in agreement with the Faxen's value for the case of two equal sized touching spheres reported in [45].

2.5. The Mobility of an Active Dimer

Once the normal shear component $\sigma_{\mu v}(\mu)$ has been obtained (see Equations (24) and (25)) the reciprocal theorem of Equation (16) can be used along with the induced slip velocity of Equations (14) and (15) and constant mobility coefficients $M_{\pm}$ to render:

$$\begin{array}{c} U_{\mathrm{d}} = \frac{1}{3f}\int_0^\infty [M_- u_-(\mu) - M_+ u_+(\mu)]\frac{\sigma_{\mu v}}{\mu}\frac{\mu d\mu}{(1+\mu^2)^2} \\ = \frac{1}{3f}\iint_0^\infty s[M_- G_-(s) - M_+ G_+(s)]\left[-\frac{\mu^2}{2(1+\mu^2)^{3/2}} + \frac{3\mu^2}{2(1+\mu^2)^{5/2}}\right]J_1(\mu s)dsd\mu, \\ + \frac{1}{3f}\iiint_0^\infty s[M_- G_-(s) - M_+ G_+(s)]I(t)J_1(\mu t)J_1(\mu s)dtdsd\mu \end{array} \quad (27)$$

where $I(t)$ is defined in Equation (25). The double integral in the right hand side of Equation (27) can be evaluated using the following two identities [40]:

$$\int_0^\infty \frac{\mu^2}{(1+\mu^2)^{3/2}}J_1(\mu s)d\mu = e^{-s}, \int_0^\infty \frac{\mu^2}{(1+\mu^2)^{5/2}}J_1(\mu s)d\mu = \frac{s}{3}e^{-s}, \quad (28)$$

and the triple integral in Equation (27) can be evaluated using [47]:

$$\int_0^\infty J_1(\mu s)J_1(\mu t)\mu d\mu = \frac{\delta(s-t)}{s}, \quad (29)$$

where $\delta(s)$ denotes the Dirac delta function.

Finally, substituting Equations (27) and (28) into Equation (27) yields:

$$\begin{array}{c} U_{\mathrm{d}} = \frac{1}{3f}\int_0^\infty [M_- G_-(s) - M_+ G_+(s)][s(s-1)e^{-s} + 2I(s)]ds \\ = \frac{4}{3f}\int_0^\infty [M_- G_-(s) - M_+ G_+(s)]\frac{s^2 \sin \mathrm{h}s}{2s+\sin \mathrm{h}(2s)}ds \end{array}, \quad (30)$$

which provides the sought analytical solution for the diffusiophoretic self-propulsion mobility of an active JD in terms of the parameters $G_{\pm}(s)$ defined in Equation (15), where $A(s)$ & $B(s)$ are the solutions of Equation (5) and I(s) is given in Equation (25).

Once the mobility U_d of the JD is explicitly obtained in Equation (30), it is then possible to express the Stokes stream function $\widetilde{\Psi}$ for the velocity field around the active dimer as;

$$\widetilde{\Psi}(\mu, v) = \frac{U_d}{2}\frac{\mu^2}{(\mu+v^2)^2} + \frac{\mu}{(\mu+v^2)^{3/2}}\int_0^\infty Q(s,v)J_1(s\mu)ds, \quad (31)$$

where in lieu of [43]:

$$Q(s,v) = \left[v\widetilde{A}(s) + \widetilde{B}(s)\right]\sin \mathrm{h}(sv) + \left[v\widetilde{C}(s) + \widetilde{D}(s)\right]\cos \mathrm{h}(sv). \quad (32)$$

The four unknown coefficients $\widetilde{A}(s)$, $\widetilde{B}(s)$, $\widetilde{C}(s)$, $\widetilde{D}(s)$ in Equation (32) are obtained by imposing the proper boundary conditions on the no-slip rigid JD surface (see Equation (14)):

$$\widetilde{\Psi}(\mu, \pm 1) = 0,\ u_\mu(\mu, \pm 1) = \frac{(1+\mu^2)^2}{\mu}\frac{\partial \widetilde{\Psi}(\mu, \pm 1)}{\partial v} = M_{\pm}\left(1+\mu^2\right)^{1/2}\int_0^\infty sG_{+-}(s)J_1(s\mu)ds. \quad (33)$$

For example, imposing the no-penetration condition in Equation (33) leads to:

$$\begin{array}{c} \widetilde{B}(s)\sin \mathrm{h}(s) + \widetilde{C}(s)\cos \mathrm{h}(s) = 0 \\ \widetilde{A}(s)\sin \mathrm{h}(s) + \widetilde{D}(s)\cos \mathrm{h}(s) = -\frac{1}{2}U_d\left(1+\frac{1}{s}\right)e^{-s}, \end{array} \quad (34)$$

Since [40]:

$$\frac{\mu^2}{(1+\mu^2)^{1/2}} = \int_0^\infty \left(1+\frac{1}{s}\right)e^{-s}J_1(\mu s)ds. \quad (35)$$

Next, in lieu of Equations (31) and (32) and the no-slip condition in Equation (33), one gets

$$\int_0^\infty \frac{\partial Q}{\partial v}(s,\pm 1)J_1(s\mu)ds = \pm\frac{3}{2}U_d\frac{\mu}{(1+\mu^2)^{3/2}} + M_\pm\int_0^\infty sG_\pm(s)J_1(s\mu)ds. \tag{36}$$

Recalling again [40] that $\mu/(1+\mu^2)^{3/2} = \int_0^\infty se^{-s}J_1(s\mu)ds$ and substituting Equation (32) in Equation (36) renders:

$$\begin{array}{c}\pm\widetilde{A}(s)[\sin h(s) + s*\cos h(s)] + \widetilde{C}(s)[\cos h(s) + s*\sin h(s)] \\ +s\left[\widetilde{B}(s)\cos h(s) + \widetilde{D}(s)\sin h(s)\right] = s\left[M_\pm G_\pm(s) \pm \frac{1}{2}U_d e^{-s}\right].\end{array} \tag{37}$$

and thus:

$$\begin{array}{c}\widetilde{A}(s)[\sin h(s) + s\cos h(s)] + s\widetilde{D}(s)\sin h(s) = \frac{s}{2}[M_+G_+(s) - M_-G_-(s) + U_d e^{-s}] \\ \widetilde{C}(s)[\cos h(s) + s\sin h(s)] + s\widetilde{B}(s)\cos h(s) = \frac{s}{2}[M_+G_+(s) + M_-G_-(s)]\end{array}. \tag{38}$$

Finally, combining Equation (34) with Equation (38) provides the following explicit solutions for the four coefficients determining the Stokes stream function of Equations (31) and (32):

$$\begin{array}{c}\widetilde{A}(s) = \frac{U_d\left(s+e^{-s}\sin h(s)\right)+s[M_+G_+(s)-M_-G_-(s)]\cos h(s)}{2s+\sin h(2s)} \\ \widetilde{B}(s) = -\frac{s[M_+G_+(s)+M_-G_-(s)]\cos h(s)}{2s-\sin h(2s)} \\ \widetilde{C}(s) = -\frac{s[M_+G_+(s)+M_-G_-(s)]\sin h(s)}{2s-\sin h(2s)} \\ \widetilde{D}(s) = -\frac{U_d\left[1+s+\left(e^{-s}/s\right)\sin h(s)\right]+s[M_+G_+(s)-M_-G_-(s)]\sin h(s)}{2s+\sin h(2s)}\end{array}. \tag{39}$$

Note that for the particular no-slip case, i.e., $M_\pm = 0$, Equation (39) reduces to the already known solution corresponding to an inert dimer given in Equation (21), where $\widetilde{B}(s) = \widetilde{C}(s) = 0$, $\widetilde{A}(s) = D(s)$, $\widetilde{D}(s) = C(s)$ and $U_d = 1$.

2.6. Infinitely Large Damköhler Number

A special interesting limiting case [16] of the above formulation is when one of the spheres is inert ($v = -1$) and the other ($v = 1$) is chemically active with an infinitely large Damköhler number ($\beta_+ \to \infty$). The corresponding boundary conditions on the solute concentration C for this case are thus given by:

$$\left.\frac{\partial C}{\partial n}\right|_{v=-1} = \left.\frac{1}{h_v}\frac{\partial C}{\partial v}\right|_{v=-1} = 0,\ C|_{v=1} = 0. \tag{40}$$

In lieu of Equation (5) one gets for ($\alpha_- = \beta_- = \alpha_+ = 0$, $\beta_+ \to \infty$) the following two equations:

$$\begin{array}{c}A(s)\cos h(s) + B(s)\sin h(s) = 0 \\ \frac{1}{\sin h(s)}\frac{d}{ds}\left(sinh^2(s)\frac{dA(s)}{ds}\right) = \frac{1}{\cos h(s)}\frac{d}{ds}\left(cosh^2(s)\frac{dB(s)}{ds}\right),\end{array} \tag{41}$$

which determine the coefficients $A(s)$ and $B(s)$. The leading-order asymptotic solution of Equation (41) for very large s is:

$$A(s) = B(s) = -e^{-2s}. \tag{42}$$

The numerical solution procedure for solving Equation (41) is given in Appendix A. It is important to note that the agreement between the numerical solution of Equation (41) and the asymptotic solution given in Equation (42) is quite good, at least for $A(s)$. Hence,

there is merit in analytically calculating the JD mobility by using the simple asymptotic solutions of Equation (42) which render:

$$G_+(s) = 0,\ G_-(s) = -8e^{-3s}. \tag{43}$$

Finally we find that the resulting JD mobility U_d in the limiting case of an infinitely large Damköhler number can be directly obtained from Equation (30) by substituting Equations (25) and (42) as:

$$U_d = -\frac{32}{3f}M_- \int_0^\infty \frac{s^2 e^{-3s} sinh(s)}{2s + \sin h(2s)} ds, \tag{44}$$

where by virtue of Equation (26) and $f = 0.645$, one gets $U_d = -0.2480 \times M_-$. This value was also validated by substituting the approximate solutions of Equation (42) into the general expression of U_d given in Equation (30) and numerically integrating Equation (30). However, if the numerical solutions for $A(s)$ and $B(s)$ are used, Equation (30) yields $U_d = -0.3261 \times M_-$. Once the dimer mobility U_d is known the stream function and flow field can be explicitly found using Equations (31), (32) and (39).

3. Results and Discussion

To illustrate the newly derived solutions for dimer mobility, two cases are initially analysed. The first case is a dimer with an upper active sphere with a fixed rate of $\beta_+ = 1$ and zero fixed flux, i.e., $\alpha_+ = 0$, while the lower sphere is inert, i.e., $\beta_- = \alpha_- = 0$. The solutions for the first derivatives of $A(s)$ and $B(s)$ are given in Figure 2, following the numerical solution of Equation (7) and using the approximate solution of Equation (9). The plot for $\mathrm{d}A/\mathrm{d}s$ is given in a log scale for better clarity. The choice of plotting the first derivatives of $A(s)$ and $B(s)$ and not $A(s)$ and $B(s)$ themselves originates from the expression for the mobility U_d of Equation (30), which mostly depends on those derivatives and less on the second derivatives according to Equation (15).

It is clear that there is a very good agreement between the numerical and approximate solutions for $s > 1$ but not for small s. Hence, the approximate solutions of Equation (9) can be seen as the outer solutions for $A(s)$ and $B(s)$, although the agreement for $\mathrm{d}B/\mathrm{d}s$ at small s can still be argued as fair.

Examining the approximate solutions of Equation (9), one can see that for $\alpha_+ = \beta_- = \alpha_- = 0$, we can rewrite the approximate solutions as:

$$A(s) = B(s) = -\frac{\beta_+}{(\beta_+ - 2)} e^{-2s}. \tag{45}$$

Hence, both approximate solutions are equal and converge to Equation (42) for $\beta_+ \to \infty$. The change of sign in $A(s)$ and $B(s)$ when β_+ becomes larger than two, should also be noted as it affects the direction of the dimer's mobility U_d given by Equation (30). However, the numerical solution of Equation (7) points to a singularity at about $\beta_+ \simeq 1.85$, where a change in the sign of U_d also occurs as discussed further on when examining Table 1.

Table 1. Mobility velocities according to Equations (7)–(9) and for the cases of Figures 2 and 3, i.e., ($\beta_+ = 1,\ \alpha_+ = \beta_- = \alpha_- = 0$) and ($\beta_+ = \beta_- = 0,\ \alpha_+ = 1,\ \alpha_- = 2$) respectively.

	Case	Equation (7), Numerical Solution	Equation (8), Exact ($\beta_\pm$=0) Solution	Equation (9), Approximate Solution
U_d^+	Figure 2	−0.09	0	0
U_d^-	Figure 2	0.4037	0	0.2480
U_d^+	Figure 3	−0.3422	−0.3423	−0.2480
U_d^-	Figure 3	−0.1391	−0.1390	−0.1240

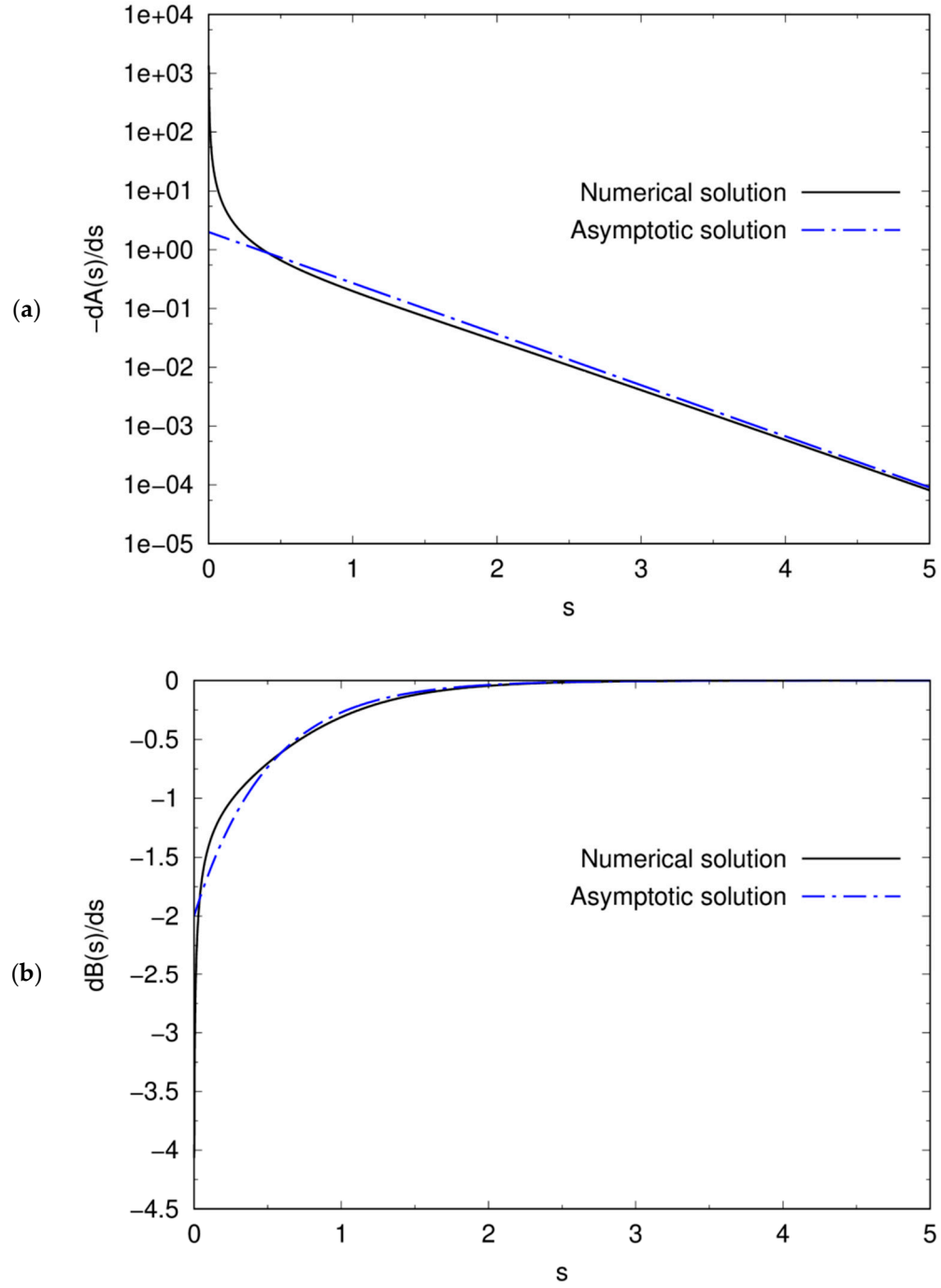

Figure 2. The variations of the first derivatives of (**a**) $A(s)$ and (**b**) $B(s)$ with s for $\beta_+ = 1$, $\alpha_+ = 0$, $\beta_- = \alpha_- = 0$ according to the numerical solution of Equation (7) and the approximate solution of Equation (9).

The second case to be studied is when both spheres have zero fixed rates, i.e., $\beta_+ = \beta_- = 0$ and different fixed fluxes, which in this particular case are $\alpha_+ = 1$, $\alpha_- = 2$. In this case the exact solution of Equation (8) holds and the solutions for the first derivatives of $A(s)$ and $B(s)$ are presented in Figure 3. Excellent agreement is achieved between the numerical solution of Equation (7) and the exact solution of Equation (8), where very good agreement between all three solutions is also achieved for $s > 1$. Nevertheless, this time the approximate solution for dB/ds at $s < 1$ does not agree well with the other solutions, reinforcing the limitation of its accuracy as an outer solution for $s > 1$.

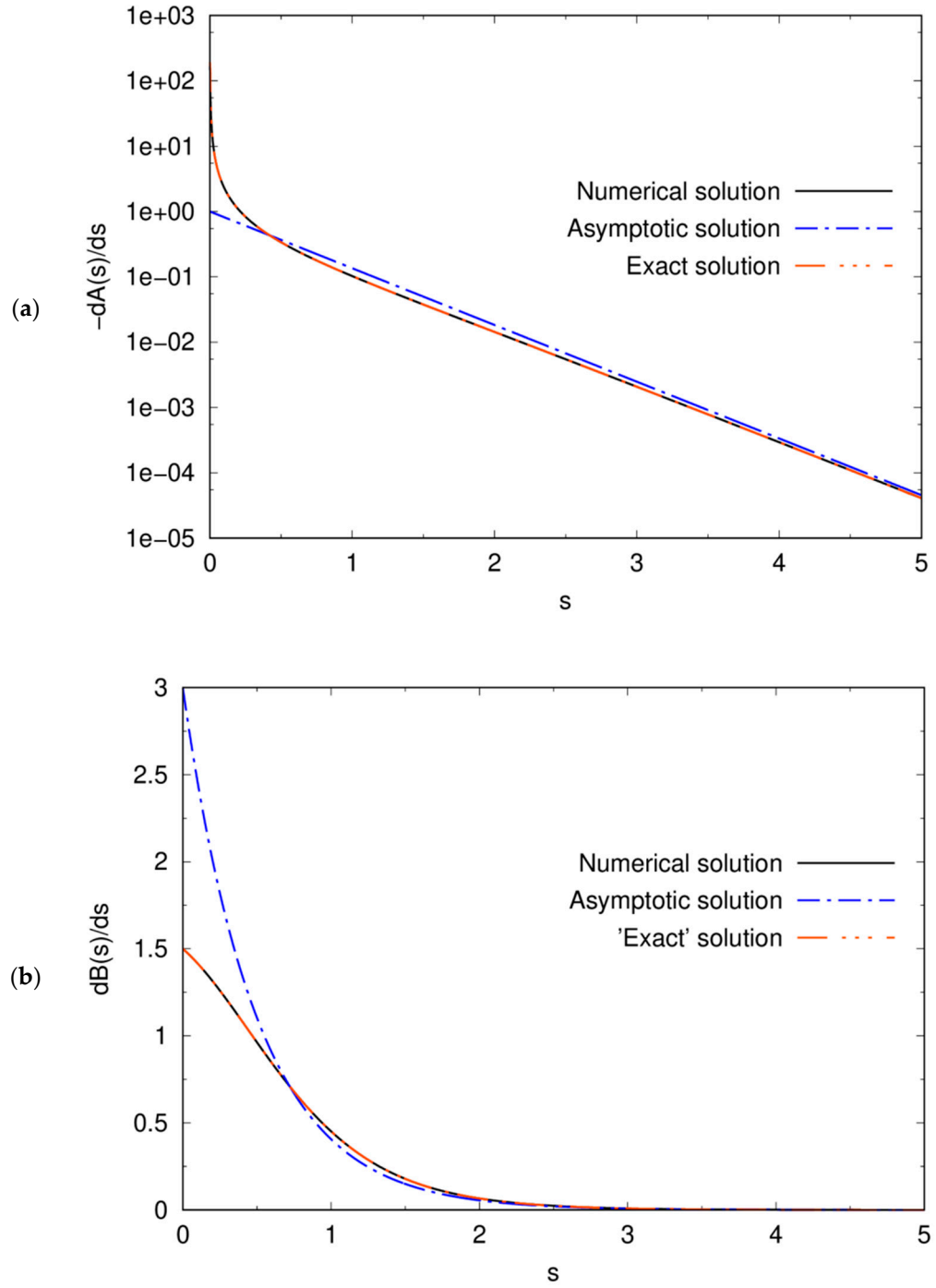

Figure 3. The variations of the first derivatives of (**a**) $A(s)$ and (**b**) $B(s)$ with s for $\beta_+ = 0$, $\alpha_+ = 1$, $\beta_- = 0$, $\alpha_- = 2$ according to the numerical solution of Equation (7), the approximate solution of Equation (9), and the exact solution of Equation (8). The numerical solution of Equation (7) and the exact solution of Equation (8) lines coincide.

Following Equation (30), the dimer's mobility U_d can be expressed as

$$U_d = U_d^+ M_+ + U_d^- M_-. \tag{46}$$

The values of U_d^+ & U_d^- are shown in Table 1 for the cases depicted in Figures 2 and 3 after performing the integration expressed in Equation (30). As expected, the exact solution according to Equation (8) agrees very well with the numerical solution for the case of

Figure 3, i.e., zero fixed rate $\beta_+ = \beta_- = 0$ and yields no mobility for the case of Figure 2, i.e., zero fixed flux $\alpha_+ = \alpha_- = 0$.

The agreement between the numerical and approximate solutions is qualitatively good as both agree concerning the proper use of the sign, but there is a difference of up to 40% in the case of Figure 2. In that case U_d^+ is almost zero. The effect of varying β_+ on the dimer mobility for the case with a lower inert sphere and an upper sphere with zero fixed flux, i.e., $\alpha_+ = \beta_- = \alpha_- = 0$ is illustrated in Figure 4. It is seen that in general $\left|U_d^-\right| \gg \left|U_d^+\right|$ particularly for low and high values of β_+. This means that the mobility is actually mostly affected by the mobility constant of the lower inert sphere M$_-$ as already seen in Section 2.6 for the case pf $\beta_+ \to \infty$. However, near the singular points (where the first is around $\beta_+ \simeq 1.85$ as discussed in the context of Figure 2), the two terms of the dimer mobility are of similar magnitude, as seen in Figure 4, for the range of $1 < \beta_+ < 10$. It should also be noted that those points of singularity usually mark a change in the signs of U_d^+ & U_d^-. The fact that the outer solution of Equation (46) points only towards the first singularity indicates that the origin of the higher singularities is from the near fields of $A(s)$ and $B(s)$. The numerical solution blows up at the points of singularity (where the matrix of Equation (A4) becomes ill conditioned), pointing to the limitation of the current theory regarding those points.

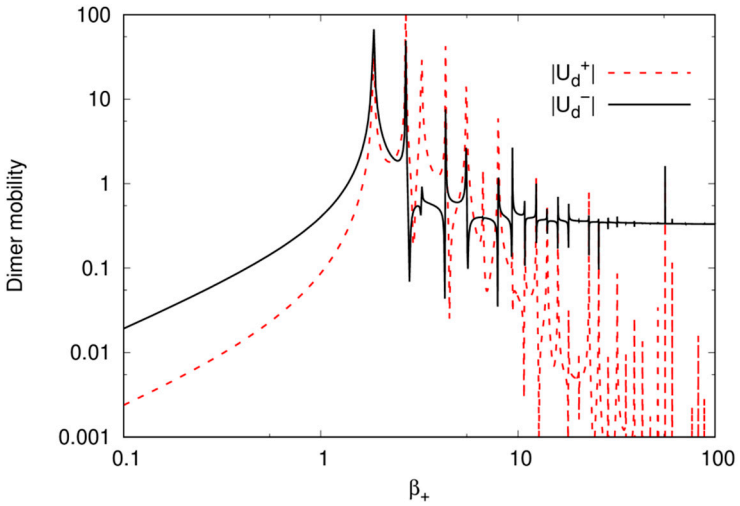

Figure 4. The variation of the dimer mobility with the upper sphere fixed-rate β_+ for the case of a dimer with a lower inert sphere and no fixed flux for the upper sphere, i.e., $\alpha_+ = \beta_- = \alpha_- = 0$, where the solution was achieved by numerically solving Equations (7) and (30).

The flow fields corresponding to Figures 2 and 3 are illustrated in Figure 5. They were calculated from the stream function formulation presented in Equation (31). This flow field is attached to the dimer, and hence the far field shows uniform flow opposite to the direction of U_d that can be calculated from Table 1, while taking $M_+ = M_- = 1$. There is not much flow activity (as relative to the dimmer) in the area between the two spheres and both flow fields show wakes both in the axial z direction and in the radial r direction, with a visible effect at a distance of at least four times the spheres' radii.

A more careful examination of the axial and radial velocity wakes shows a symmetric axial wake as one may expect from the Stokes flow with the same rate of velocity recovery for both cases. The universal behaviour of the far field of the normalised wake recovery is typical to Stokes flow as already known for a particle of an arbitrary shape embedded in free steam [48]. The axial wake is somewhat shorter, but one can conclude that at about a distance of three times the sphere's diameter (the diameter is considered as one in these plots), the velocity recovery is almost complete.

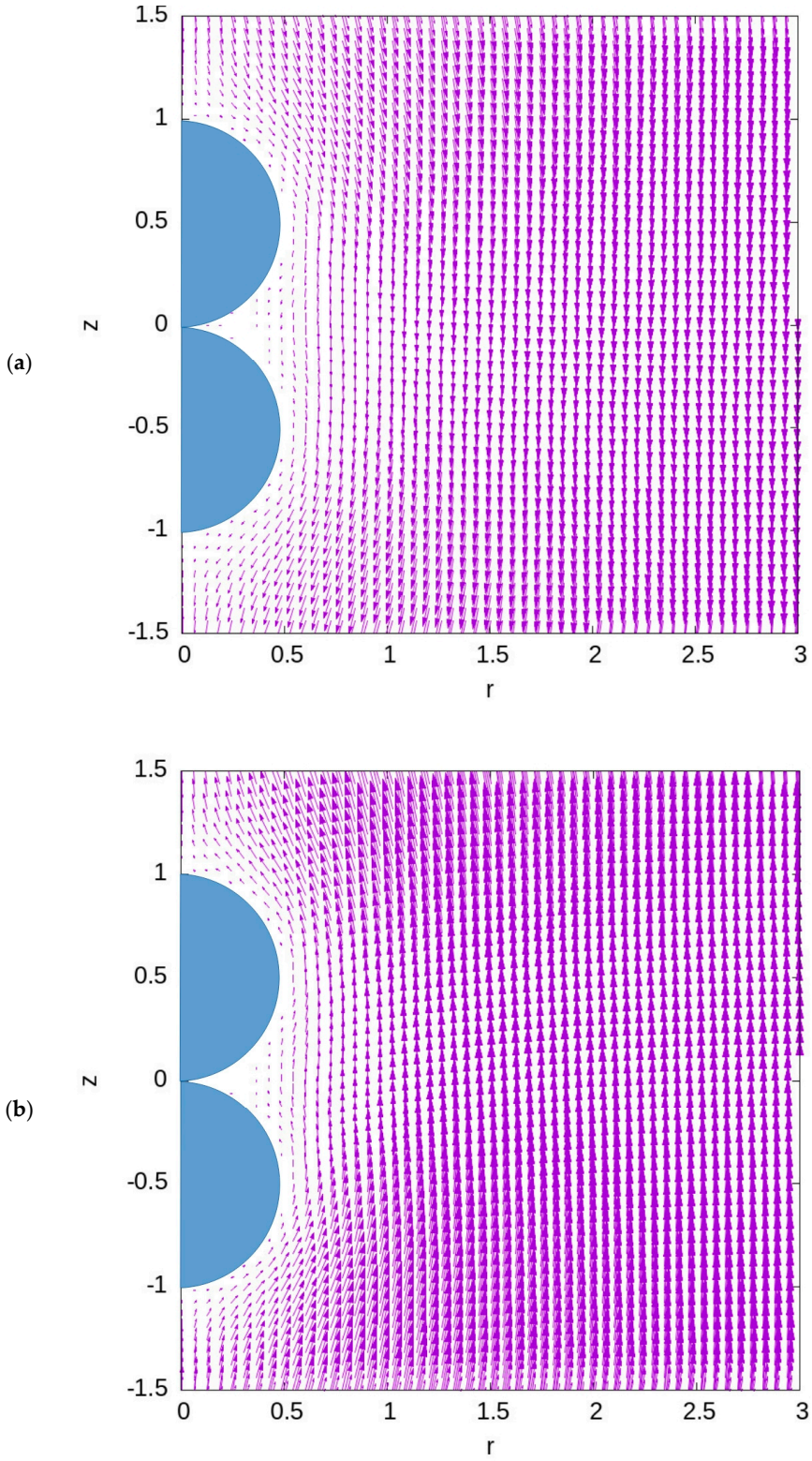

Figure 5. The velocity vector field around the dimer for the cases of (**a**) Figure 2 and (**b**) Figure 3, where $M_+ = 1$, $M_- = 1$ and the vector's length was rescaled for clarity.

This wake recovery has a consequence when one wants to use the developed theory as a sub grid scale model for simulating the motions of several interacting dimers. This is because the theory assumes a single dimer suspended in a free space (i.e., neglecting the effect of nearby dimers), hence the implementation will be limited to a dilute mixture of dimers in the medium. As a rule of thumb, one may check that the average distance

between dimers is not smaller than six times the sphere's diameter for the accuracy of using this new developed theory as a sub grid model in a larger simulation, when it comes to dimers of the properties investigated in Figures 2 and 3.

Finally, for completeness we show the variations of the first derivatives of the functions $A(s)$ & $B(s)$ in Figure 6, for the case of Section 2.6, i.e., the upper sphere having an infinite Damköhler number $(\beta_+ \to \infty)$ and the lower sphere being inert. We see that the agreement for $\mathrm{d}A/\mathrm{d}s$ is very good between the asymptotic solution of Equation (42) and the numerical solution for all ranges of s. However, the agreement for $\mathrm{d}B/\mathrm{d}s$ is very good only for $s > 1$. This explains the difference of about 24% found between the approximate and numerical values for U_d as expressed at the end of Section 2.6. The flow fields showed similar patterns to the previously discussed cases, and thus for the sake of brevity it is not further discussed here.

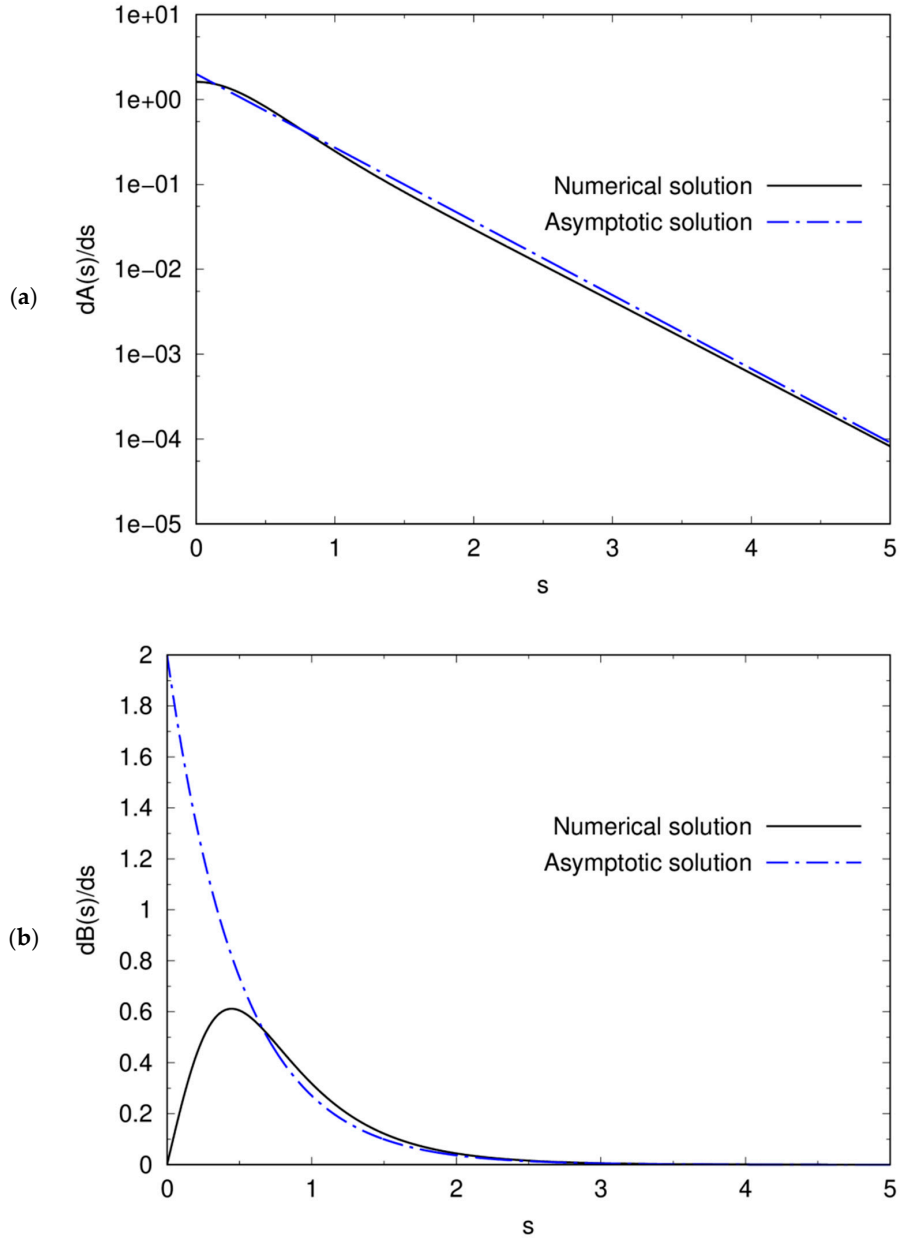

Figure 6. The variations of (**a**) $A(s)$ and (**b**) $B(s)$ with s for the case of a lower inert sphere and an upper sphere with an infinitely large Damköhler number $(\beta_+ \to \infty)$, according to the numerical solution of Equation (41) and the approximate solution of Equation (42).

4. Conclusions

A chemically active dimer consisting of two geometrically equal touching spherical colloids with different fixed fluxes and fixed rates for solute concentration was considered as it moves in a free space. New analytical solutions have been derived using two auxiliary functions $A(s)$ and $B(s)$ to compute the dimer mobility and the flow field around it. Approximate solutions were derived for both $A(s)$ and $B(s)$ which were revealed to be generally accurate as outer solutions when compared with the numerical solutions or the exact analytical solutions that were available for a dimer with no fixed-rate reaction. In the case of an upper sphere with a fixed-rate β_+ and an inert lower sphere, the dimer mobility was found to be highly dependent on the mobility constant of the lower inert sphere M-. However, points of singularity in the newly developed solutions were also found, where the first point is indicated by the approximate outer solutions of $A(s)$ and $B(s)$. At those points the assumption of linearity used in this study may become questionable, and further investigation is required. What is clear is that besides the first point of singularity, other singularities at higher s occur due to the inner solutions of $A(s)$ and $B(s)$, pointing to a merit in developing analytical inner solutions for $A(s)$ and $B(s)$ in the future.

The presented numerical procedure makes it an attractive candidate as a sub grid scale model for a multi-scale simulation of a mixture of dimers. The numerical procedure is rapid and should be easily implemented as long as the dimer's properties make it far from the points of singularity discussed earlier. The assumption of a dimer embedded in a free space, limits this application for dilute mixture of dimers, where a simple rule of thumb was suggested of keeping an average distance of at least about six times the sphere's diameter between the dimers. The effect of nearby walls or other boundaries can also be important. This is not modelled in this study, but it can be analysed, for example using the image method. The effect of a nearby wall may become significant when the dimer is at a distance from the wall of less than three times the sphere's diameter.

Author Contributions: Conceptualization, T.M.; Methodology, E.J.A. and T.M.; Software, E.J.A.; Validation, E.J.A.; Formal analysis, E.J.A. and T.M.; Investigation, E.J.A. and T.M.; Data curation, E.J.A.; Writing—original draft, E.J.A. and T.M.; Visualization, E.J.A.; Funding acquisition, E.J.A. and T.M. All authors have read and agreed to the published version of the manuscript.

Funding: The funding of UUKi & DBEIS grant 1011 is kindly acknowledged. EJA also acknowledges the support of the British Council Wohl Clean Growth Alliance grant 4503250561 and TM acknowledges partial support from BSF grant 2018168.

Data Availability Statement: Data are available upon request to the authors.

Conflicts of Interest: The authors declare no conflict of interest.

Abbreviations

List of main symbols

$A(s)$	Auxiliary function defined in Equation (4) and governed by Equation (7)
$\widetilde{A}(s)$	Stream-function coefficient defined in Equation (32) and found in Equation (39) for active dimer
a	Radius of the sphere, normalised to $\frac{1}{2}$.
$B(s)$	Auxiliary function defined in Equation (4) and governed by Equation (7)
$\widetilde{B}(s)$	Stream-function coefficient defined in Equation (32) and found in Equation (39) for active dimer
C	Solute concentration
$C(s)$	Stream-function coefficient defined in Equation (20) and found in Equation (21) for inert dimer
$\widetilde{C}(s)$	Stream-function coefficient defined in Equation (32) and found in Equation (39) for active dimer

D_v	Drag
$D(s)$	Stream-function coefficient defined in Equation (20) and found in Equation (21) for inert dimer
$\widetilde{D}(s)$	Stream-function coefficient defined in Equation (32) and found in Equation (39) for active dimer
$F(s)$	Auxiliary function defined in Equation (12)
f	Faxen's value of about 0.645
$G(s)$	Auxiliary function defined in Equation (15) and used to compute the dimer mobility in Equation (30)
J_n	Bessel function of the first kind and of n order
K	Dynamic viscosity
k	Diffusivity
M	Mobility coefficient of the sphere
n	Unit direction normal to the sphere
p	Pressure
r	Polar radial direction
S	Surface area of the sphere
s	Integration variable, e.g., Equation (4)
U_d	Dimer mobility, computed in Equation (30)
$\vec{u}$	Velocity vector
z	Axial (axisymmetry) co-ordinate, see Figure 1
α	Sphere's fixed-flux reaction
β	Sphere's fixed-rate reaction
μ	Tangential-sphere system co-ordinate, defined in Equation (3)
σ	Shear tensor
v	Tangential-sphere system co-ordinate, defined in Equation (3)
Ψ	Stream function of the inert dimer
$\widetilde{\Psi}$	Stream function of the active dimer
$(\,)_+$	A property that belongs to the upper sphere
$(\,)_-$	A property that belongs to the lower sphere
JD	Janus dimer

Appendix A. Numerical Solutions for the Functions $A(s)$ and $B(s)$

In order to numerically solve Equation (7), the concept of staggered central finite difference is used as follows:

$$\frac{d}{ds}\left[s \times sinh^2(s)\frac{dA(s)}{ds}\right]_i \Delta s = s_{i+0.5} \times sinh^2(s_{i+0.5})\left.\frac{dA(s)}{ds}\right|_{i+0.5} - s_{i-0.5} \times sinh^2(s_{i-0.5})\left.\frac{dA(s)}{ds}\right|_{i-0.5}, \quad \text{(A1)}$$

where $\Delta s = s_{i+0.5} - s_{i-0.5}$. Hence, discretising Equation (7a) using a uniform grid leads to:

$$\begin{array}{c} s_{i+0.5} \times sinh^2(s_{i+0.5})(A_{i+1} - A_i) - s_{i-0.5} \times sinh^2(s_{i-0.5})(A_i - A_{i-1}) \\ + \frac{\beta_+ - \beta_-}{4} sinh(2s_i)\Delta s^2 A_i + \frac{\beta_+ + \beta_-}{2} sinh^2(s_i)\Delta s^2 B_i = \frac{(\alpha_+ - \alpha_-) - (\beta_+ - \beta_-)}{2} e^{-s} sinh(s_i)\Delta s^2, \end{array} \quad \text{(A2)}$$

where I = 1, 2, …, N. Taking that $s_1 = \Delta s/2$ means that the value of A_0 does not affect the solution of Equation (A2) (as long as $A(s)$ has a singularity up to $1/s^2$). Similarly the discretised Equation (7b) can be written as:

$$\begin{array}{c} s_{i+0.5} \times cosh^2(s_{i+0.5})(B_{i+1} - B_i) - s_{i-0.5} \times cosh^2(s_{i-0.5})(B_i - B_{i-1}) \\ + \frac{\beta_+ - \beta_-}{4} sinh(2s_i)\Delta s^2 B_i + \frac{\beta_+ + \beta_-}{2} cosh^2(s_i)\Delta s^2 A_i = \frac{(\alpha_+ - \alpha_-) - (\beta_+ - \beta_-)}{2} e^{-s} cosh(s_i)\Delta s^2, \end{array} \quad \text{(A3)}$$

Again, taking that $s_1 = \Delta s/2$ means that the value of B_0 does not affect the solution of Equation (A3) (as long as $B(s)$ has a singularity lower than $1/s$). For a very large s the boundary conditions for Equations (A2) and (A3) can be taken as $A_{N+1} = A_N e^{-2\Delta s}$, $B_{N+1} = B_N e^{-2\Delta s}$ respectively, following Equation (9).

Equations (A2) and (A3) can be rewritten as a block tri-diagonal matrix equation as follows:

$$\begin{pmatrix} \overline{\overline{b}}_1 & \overline{\overline{c}}_1 & 0 & 0 & 0 & 0 & 0 \\ \overline{\overline{a}}_2 & \overline{\overline{b}}_2 & \overline{\overline{c}}_2 & 0 & 0 & 0 & 0 \\ 0 & \ddots & \ddots & \ddots & 0 & 0 & 0 \\ 0 & 0 & \overline{\overline{a}}_i & \overline{\overline{b}}_i & \overline{\overline{c}}_i & 0 & 0 \\ 0 & 0 & 0 & \ddots & \ddots & \ddots & 0 \\ 0 & 0 & 0 & 0 & \overline{\overline{a}}_{N-1} & \overline{\overline{b}}_{N-1} & \overline{\overline{c}}_{N-1} \\ 0 & 0 & 0 & 0 & 0 & \overline{\overline{a}}_N & \overline{\overline{b}}_N \end{pmatrix} \begin{pmatrix} \overline{X}_1 \\ \overline{X}_2 \\ \vdots \\ \overline{X}_i \\ \vdots \\ \overline{X}_{N-1} \\ \overline{X}_N \end{pmatrix} = \begin{pmatrix} \overline{F}_1 \\ \overline{F}_2 \\ \vdots \\ \overline{F}_i \\ \vdots \\ \overline{F}_{N-1} \\ \overline{F}_N \end{pmatrix}, \tag{A4}$$

where,

$$\overline{\overline{a}}_i = \begin{pmatrix} s_{i-0.5} \times sinh^2(s_{i-0.5}) & 0 \\ 0 & s_{i-0.5} \times cosh^2(s_{i-0.5}) \end{pmatrix}, \; i = 2 \cdots N, \tag{A5}$$

$$\overline{\overline{c}}_i = \begin{pmatrix} s_{i+0.5} \times sinh^2(s_{i+0.5}) & 0 \\ 0 & s_{i+0.5} \times cosh^2(s_{i+0.5}) \end{pmatrix}, \; i = 1 \cdots N, \tag{A6}$$

$$\overline{\overline{b}}_i = \begin{pmatrix} \frac{\beta_+ - \beta_-}{4} sinh(2s_i)\Delta s^2, & \frac{\beta_+ + \beta_-}{2} sinh^2(s_i)\Delta s^2 \\ \frac{\beta_+ + \beta_-}{2} cosh^2(s_i)\Delta s^2, & \frac{\beta_+ - \beta_-}{4} sinh(2s_i)\Delta s^2 \end{pmatrix} - \overline{\overline{a}}_i - \overline{\overline{c}}_i \left[1 - e^{-2\Delta s} \times \Theta(N - 0.5)\right], \; i = 1 \cdots N, \tag{A7}$$

$$\overline{X}_i = \begin{pmatrix} A_i \\ B_i \end{pmatrix}, \; \overline{F}_i = \begin{pmatrix} \frac{(\alpha_+ - \alpha_-) - (\beta_+ - \beta_-)}{2} e^{-s} sinh(s_i)\Delta s^2 \\ \frac{(\alpha_+ - \alpha_-) - (\beta_+ - \beta_-)}{2} e^{-s} cosh(s_i)\Delta s^2 \end{pmatrix}, \; i = 1 \cdots N. \tag{A8}$$

$\overline{\overline{a}}_1 = 0$ and $\Theta(N - 0.5)$ is the step function. Equation (A4) can be solved using the block Thomas algorithm [41].

Equation (41) can be discretised in a similar manner yielding:

$$\overline{\overline{a}}_i = \begin{pmatrix} 0 & 0 \\ sinh^2(s_{i-0.5}) & -\tan h(s_i) cosh^2(s_{i-0.5}) \end{pmatrix}, \; i = 2 \cdots N, \tag{A9}$$

$$\overline{\overline{c}}_i = \begin{pmatrix} 0 & 0 \\ sinh^2(s_{i+0.5}) & -\tan h(s_i) cosh^2(s_{i+0.5}) \end{pmatrix}, \; i = 1 \cdots N, \tag{A10}$$

$$\overline{\overline{b}}_i = \begin{pmatrix} 1, & \tan h(s_i) \\ 0, & 0 \end{pmatrix} - \overline{\overline{a}}_i - \overline{\overline{c}}_i \left[1 - e^{-2\Delta s} \times \Theta(N - 0.5)\right], \; i = 1 \cdots N, \tag{A11}$$

$$\overline{X}_i = \begin{pmatrix} A_i \\ B_i \end{pmatrix}, \; \overline{F}_i = \begin{pmatrix} -e^{-s}/\cos h(s_i) \\ 0 \end{pmatrix}, \; i = 1 \cdots N, \tag{A12}$$

where Equation (41) was divided by cosh(*s*) and Equation (42) was multiplied by sinh(*s*) before discretisation. The matrix equation again can be solved using the block Thomas algorithm.

References

1. Bishop, K.J.; Biswal, S.L.; Bharti, B. Active colloids as models, materials, and machines. *Annu. Rev. Chem. Biomol. Eng.* **2023**, *14*, 1–30. [CrossRef]
2. Michelin, S. Self-Propulsion of Chemically Active Droplets. *Annu. Rev. Fluid Mech.* **2023**, *55*, 77–101. [CrossRef]
3. Moran, J.K.; Posner, J.D. Phoretic self-propulsion. *Annu. Rev Fluid Mech.* **2017**, *49*, 511–540. [CrossRef]
4. Fusi, A.D.; Li, Y.; Llopis-Lorento, A.; Partino, T.; Van Hest, J.C.M. Achieving control in micro/nano motor mobility. *Angew. Chen. Ind. Ed.* **2022**, *62*, 14754.
5. Wang, Q.; Jim, D. Active micro/nanoparticles in colloidal micro-swarms. *Nanomaterial* **2023**, *13*, 1687. [CrossRef]
6. Golestanian, R.; Liverpool, T.B.; Ajdari, A. Propulsion of a Molecular Machine by Asymmetric Distribution of Reaction Products. *Phys. Rev. Lett.* **2005**, *94*, 220801. [CrossRef]
7. Golestanian, R.; Liverpool, T.B.; Ajdari, A. Designing phoretic micro- and nano-swimmers. *New J. Phys.* **2007**, *9*, 126. [CrossRef]
8. Michelin, S.; Lauga, E. Phoretic self-propulsion of finite Péclet numbers. *J. Fluid Mech.* **2014**, *747*, 572–602. [CrossRef]
9. Ebbens, S.; Tu, M.H.; Howe, J.R.; Golestanian, R. Size dependence of the propulsion velocity for catalytic Janus-sphere swimmers. *Phys. Rev. E* **2012**, *85*, 020401. [CrossRef]

10. Popescu, M.N.; Uspal, W.E.; Dietrich, S. Self-diffusiophoresis of chemically active colloids. *Eur. Phys. J. Spec. Top.* **2016**, *225*, 2189–2206. [CrossRef]
11. Reigh, S.Y.; Huang, M.-J.; Schofield, J.; Kapral, R. Microscopic and continuum descriptions of Janus motor fluid flow fields. *Philos. Trans. R. Soc. A* **2016**, *374*, 20160140. [CrossRef]
12. Upsal, W.E. Theory of light-activated catalytic Janus particles. *J. Chem. Phys.* **2019**, *150*, 114902.
13. Avital, E.J.; Miloh, T. Self-thermophoresis of laser-heated spherical Janus particles. *Eur. Phys. J. E* **2021**, *44*, 139. [CrossRef]
14. Lei, L.; Cheng, R.; Zhou, Y.; Yang, T.; Liang, B.; Wang, S.; Zhang, X.; Lin, G.; Zhou, X. Estimating the velocity of chemically-driven Janus colloids considering the anisotropic concentration field. *Front. Chem.* **2022**, *10*, 97361. [CrossRef]
15. Masoud, H.; Rothenstein, J.R. Diffusive mass transfer from a Janus sphere. *Phys. Rev. Fluids* **2022**, *7*, 070501. [CrossRef]
16. Davis, A.M.J.; Yariv, E. Self-diffusiophoresis of Janus particle at large Damköhler number. *J. Eng. Math.* **2022**, *133*, 5. [CrossRef]
17. Leshansky, A.M.; Kenneth, O.; Gat, O.; Avron, J.E. A frictionless micro swimmer. *New J. Phys.* **2007**, *9*, 147. [CrossRef]
18. Popescu, M.N.; Dietrich, S.; Tasinkevych, M.; Ralston, J. Phoretic motion of spheroidal particles due to self-generated solute gradients. *Eur. Phys. J. E* **2010**, *31*, 351–367. [CrossRef] [PubMed]
19. Michelin, S.; Lauga, E. Geometric tuning of self-propulsion for Janus catalytic particles. *Sci. Rep.* **2017**, *7*, 42264. [CrossRef] [PubMed]
20. Miloh, T.; Nagler, J. Light-induced self thermophoresis of Janus spheroidal particles. *Electrophoresis* **2018**, *39*, 2417–2424. [CrossRef] [PubMed]
21. Yariv, E. Self-diffusiophoresis of slender catalytic colloids. *Langmuir* **2019**, *36*, 6903–6915. [CrossRef] [PubMed]
22. Shemi, D.; Solomon, M.J. Self-propulsion and active motion of Janus ellipsoids. *J. Phys. Chem. B* **2018**, *122*, 10247–10255. [CrossRef] [PubMed]
23. Dean, V.S.; Kim, D.O.; Snoeyink, C.; Sun, Y.; Shih, S. Shape and orientation-dependent diffusiophoresis of colloidal ellipsoids. *Phys. Rev. E* **2023**, *107*, 2052602. [CrossRef]
24. Fair, M.C.; Anderson, J.L. Electrophoresis of non-uniformly charged ellipsoidal particles. *J. Colloid Interface Sci.* **1989**, *127*, 388–400. [CrossRef]
25. Stone, H.A.; Samuel, A.P.T. Propulsion of microorganisms by surface distortions. *Phys. Rev. Lett.* **1986**, *77*, 19. [CrossRef]
26. Popescu, M.N.; Tasinkevych, M.; Dietrich, S. Pulling and pushing a cargo with a catalytically active carrier. *Europhys. Lett.* **2011**, *95*, 28004. [CrossRef]
27. Reigh, S.K.; Karpal, S. Catalytic dimer nano-motors continuum theory and microscopic dynamics. *Soft Matt.* **2015**, *11*, 3149. [CrossRef] [PubMed]
28. Michelin, S.; Lauga, E. Autophoretic locomotion from geometric asymmetry. *Eur. Phys. J. E* **2015**, *38*, 7. [CrossRef] [PubMed]
29. Nasouri, B.; Golestanian, R. Exact axisymmetric interaction of phoretically active Janus particles. *J. Fluid Mech.* **2020**, *905*, A13. [CrossRef]
30. Lisicki, M.; Reigh, S.Y.; Lauga, E. Autophoretic motion in three dimensions. *Soft Matter* **2018**, *14*, 3304–3314. [CrossRef]
31. Moon, F.; Spencer, D.E. *Field Theory Handbook*; Springer: Berlin/Heidelberg, Germany, 1990.
32. Miloh, T.; Avital, E.J. Travelling-wave electrophoresis, electro-hydrodynamics, electro-rotation and symmetry-breaking of a polarizable dimer in nonuniform fields. *Micromachines* **2022**, *13*, 473. [CrossRef] [PubMed]
33. Wang, Z.; Mu, Y.; Lyn, D.; Wu, M.; Li, Z.; Wong, Z.; Wang, Y. Engineering shapes of active colloids for tunable dynamics. *Curr. Opin. Colloid Interface Sci.* **2022**, *61*, 101608. [CrossRef]
34. Domínguez, A.; Popescu, M.N. A fresh view on phoresis and self-phoresis. *Curr. Opin. Colloid Interface Sci.* **2022**, *61*, 101610. [CrossRef]
35. Hu, Y.; Liu, W.; Sun, Y. Self-propelled micro/nanonmeters "on the move" platforms: Cleaners, sensors and reactors. *Adv. Funct. Mater.* **2022**, *32*, 2109181. [CrossRef]
36. Li, K.; Ma, K. Rotation and Retention Dynamics of Rod-Shaped Colloids with Surface Charge Heterogeneity in Sphere-in-Cell Porous Media Model. *Langmuir* **2019**, *35*, 5471–5483. [CrossRef]
37. Gomez-Flores, A.; Bradford, S.A.; Hwang, G.; Heyes, G.W.; Kim, H. Particle–bubble interaction energies for particles with physical and chemical heterogeneities. *Miner. Eng.* **2020**, *155*, 106472. [CrossRef]
38. Drelich, J.; Wang, Y.U. Charge heterogeneity of surfaces: Mapping and effects on surface forces. *Adv. Colloid Interface Sci.* **2011**, *165*, 91–101. [CrossRef] [PubMed]
39. Anderson, J.L. Diffuse-interface methods in fluid mechanics. *Annu. Rev. Fluid Mech.* **1989**, *30*, 139. [CrossRef]
40. Gradshteyn, I.S.; Ryzhik, I.M. *Tables of Integrals, Series and Products*; Academic Press Inc.: San Diego, CA, USA, 1980.
41. Press, W.H.; Teukolsky, S.A.; Vetterling, W.T.; Flannery, B.P. *Numerical Recipes, the Art of Scientific Computing*; Cambridge University Press: Cambridge, UK, 2007.
42. Stimson, M.; Jeffrey, G.B. The motion of two spheres in a viscous fluid. *Proc. R. Soc. A* **1926**, *111*, 110–116.
43. Cooley, M.D.; O'Neil, M.E. On the slow motion of two spheres in contact along their line of centres through a viscous fluid. *Math. Proc. Camb. Philos. Soc.* **1969**, *66*, 407–415. [CrossRef]
44. Rouse, H. *Advanced Mechanics of Fluids*; John Wiley & Sons: New York, NY, USA, 1959.
45. Happel, J.; Brenner, H. *Low Reynolds Hydrodynamics*; Martinus Nijhoff: The Hauge, The Netherlands, 1983.
46. Leshansky, A.M.; Kenneth, D. Surface tank treading: Propulsion of Purcell's toroidal swimmer. *Phys. Fluids* **2008**, *20*, 063104. [CrossRef]

47. Arfken, G.B.; Weber, H.J. *Mathematical Methods for Physicist*, 6th ed.; Elsevier: Oxford, UK, 2005.
48. Batchelor, G.K. *An Introduction to Fluid Dynamics*; Cambridge University Press: Cambridge, UK, 1992.